

# Positive longitudinal spin magnetoconductivity in $\mathbb{Z}_2$ topological Dirac semimetals

Ming-Xun Deng<sup>1</sup>, Yan-Yan Yang<sup>1</sup>, Wei Luo<sup>2</sup>, R. Ma<sup>3</sup>, Rui-Qiang Wang<sup>1,\*</sup>, L. Sheng<sup>4,5,†</sup> and D. Y. Xing<sup>4,5</sup>

<sup>1</sup>*Guangdong Provincial Key Laboratory of Quantum Engineering and Quantum Materials, GPETR Center for Quantum Precision Measurement, SPTE, South China Normal University, Guangzhou 510006, China*

<sup>2</sup>*School of Science, Jiangxi University of Science and Technology, Ganzhou 341000, China*

<sup>3</sup>*Jiangsu Key Laboratory for Optoelectronic Detection of Atmosphere and Ocean, Nanjing University of Information Science and Technology, Nanjing 210044, China*

<sup>4</sup>*National Laboratory of Solid State Microstructures and Department of Physics, Nanjing University, Nanjing 210093, China*

<sup>5</sup>*Collaborative Innovation Center of Advanced Microstructures, Nanjing University, Nanjing 210093, China*

Recently, a class of Dirac semimetals, such as  $\text{Na}_3\text{Bi}$  and  $\text{Cd}_2\text{As}_3$ , are discovered to carry  $\mathbb{Z}_2$  monopole charges. We present an experimental mechanism to realize the  $\mathbb{Z}_2$  anomaly in regard to the  $\mathbb{Z}_2$  topological charges, and propose to probe it by magnetotransport measurement. In analogy to the chiral anomaly in a Weyl semimetal, the acceleration of electrons by a spin bias along the magnetic field can create a  $\mathbb{Z}_2$  charge imbalance between the Dirac points, the relaxation of which contributes a measurable positive longitudinal spin magnetoconductivity (LSMC) to the system. The  $\mathbb{Z}_2$  anomaly induced LSMC is a spin version of the longitudinal magnetoconductivity (LMC) due to the chiral anomaly, which possesses all characters of the chiral anomaly induced LMC. While the chiral anomaly in the topological Dirac semimetal is very sensitive to local magnetic impurities, the  $\mathbb{Z}_2$  anomaly is found to be immune to local magnetic disorder. It is further demonstrated that the quadratic or linear field dependence of the positive LMC is not unique to the chiral anomaly. Base on this, we argue that the periodic-in- $1/B$  quantum oscillations superposed on the positive LSMC can serve as a fingerprint of the  $\mathbb{Z}_2$  anomaly in topological Dirac semimetals.

Topological semimetals are novel quantum states of matter, where the conduction and valence bands touch, near the Fermi level, at certain discrete momentum points or lines [1–6]. The gap-closing points or lines are protected either by crystalline symmetry or topological invariants [7–9]. A topological Dirac semimetal hosts stable gap-closing points called the Dirac points (DPs), which, in addition to the time-reversal (TR) and spatial-inversion (SI) symmetries, are protected by the crystalline symmetry. By breaking the TR or SI symmetry, a single DP can split into a pair of Weyl nodes, leading to the topological transition from a Dirac to a Weyl semimetal [10–15]. The Weyl nodes always come in pairs with opposite chiralities in momentum space, protected by topological invariants associated with the Chern flux and connected by the nonclosed Fermi-arc surface states [16–18].

The Fermi-arc surface states are regarded as the most distinctive observable spectroscopic feature of Weyl semimetals. However, their observation is sometime limited by spectroscopic resolutions. Therefore, there is an urgency to find similar smoking-gun features of Weyl semimetals in response, especially in transport measurements. Of particular interest is the transport related to the chiral anomaly, i.e., the violation of the separate number conservation laws of Weyl fermions of different chiralities. Nonorthogonal electric and magnetic fields can pump Weyl fermions between Weyl nodes of opposite chiralities, and create a population imbalance between them. The relaxation of the chirality population imbalance contributes an extra electric current to the system, which results in a very unusual positive lon-

gitudinal magnetoconductivity (LMC) [19–21]. While the positive LMC, as a condensed-matter manifestation of the chiral anomaly, was observed recently in Weyl semimetal TaAs [3, 19]. It was also observed in Dirac semimetals  $\text{Na}_3\text{Bi}$ [2, 4] and  $\text{Cd}_2\text{As}_3$ [5, 22, 23]. It is now understood that  $\text{Na}_3\text{Bi}$  and  $\text{Cd}_2\text{As}_3$ , protected by a non-trivial  $\mathbb{Z}_2$  topological invariant, belong to a new class of Dirac semimetals, in which the DPs occur in pairs and separate in momentum space along a rotation axis [7–9]. The momenta of the Dirac fermions in these Dirac semimetals are locked to their spin and orbital parity, simultaneously. The Weyl nodes at the same DP belonging to different irreducible representations in spin subspace cannot be coupled, and have to seek for a partner with the same spin from the other DP. As a consequence, the two DPs composing of two pairs of Weyl nodes are connected by two Fermi arcs [24, 25], much like in the Weyl semimetals [18].

Naturally, one may ask, in analogy to the chiral anomaly, whether there exists  $\mathbb{Z}_2$  anomaly in regard to the  $\mathbb{Z}_2$  topological charge. If there exists, how it manifests in experiments, or how to identify the  $\mathbb{Z}_2$  anomaly? In Ref. [26], by introducing a fictitious spin gauge field which couples antisymmetrically to the spin, Burkov and Kim answered the first question in the affirmative. In this paper, we present an experimental mechanism to realize the  $\mathbb{Z}_2$  anomaly for Dirac semimetals carrying the  $\mathbb{Z}_2$  monopole charges, such as  $\text{Na}_3\text{Bi}$  and  $\text{Cd}_2\text{As}_3$ , and then we propose to probe the  $\mathbb{Z}_2$  anomaly by magnetotransport measurement. As we show, the  $\mathbb{Z}_2$  anomaly, in fact, is a spin version of the chiral anomaly, in which the acceleration of electrons by a spin bias along the mag-

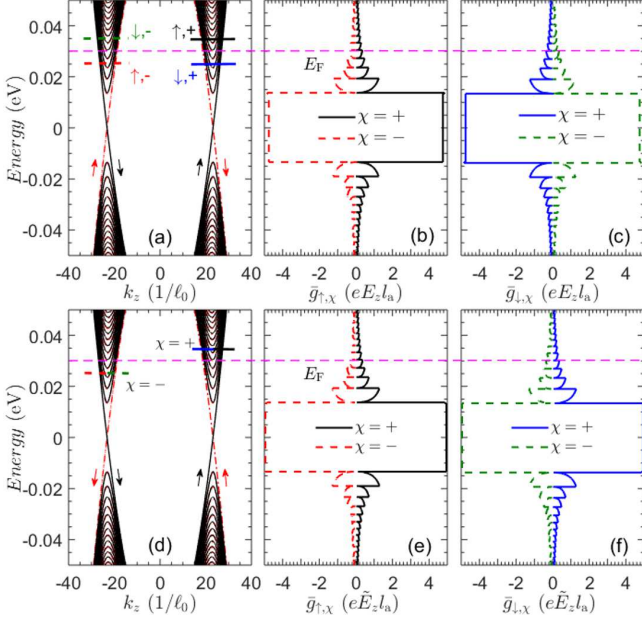


FIG. 1. The nonequilibrium local chemical potential induced by the external fields, with the upper panel for  $\nabla\mu_s = -eE_z\hat{e}_z$  and the lower panel for  $\nabla\mu_s = -es\hat{E}_z\hat{e}_z$ . The first column displays the LLs for spin- $\uparrow$  (dark-solid) and spin- $\downarrow$  (red-dash-dotted) Weyl fermions, where the parallel short lines are an enlarged illustration of the nonequilibrium local chemical potential of each Weyl valleys due to the effect of chiral and  $\mathbb{Z}_2$  anomalies. The arrows denote the driven directions of the Weyl fermions in the dispersion by the external fields and  $1/\ell_0 = \sqrt{\frac{e(B=1T)}{\hbar}}$  is unit of momentum. The last two columns, carried out for  $\text{Na}_3\text{Bi}$ [24], are numerical solutions of Eq. (5), where  $l_a \equiv \tilde{v}_F\tau_{\text{intra}}$  represents the intravalley relaxation length. Other parameters are chosen as  $B = 1T$ ,  $\tau_{\text{inter}}^c = 5\tau_{\text{intra}}^s$ ,  $\tau_{\text{intra}}^s = 20\tau_{\text{inter}}^c$  and  $\tau_{\text{inter}}^s = 100\tau_{\text{inter}}^c$ .

netic field can create carrier density imbalance between the DPs, the relaxation of which leads to a measurable positive longitudinal spin magnetoconductivity (LSMC). We further demonstrate that the  $B^2$  or  $B$  dependence emerging in the positive LMC are not unique to the chiral anomaly. Like the quantum oscillations of the positive LMC in Weyl semimetals [20, 27], we argue that the periodic-in- $1/B$  quantum oscillations superposed on the positive LSMC are remarkable fingerprint of the  $\mathbb{Z}_2$  anomaly in topological Dirac semimetals.

We start from the general low-energy Hamiltonian for topological Dirac semimetals  $\text{Na}_3\text{Bi}$  [24] and  $\text{Cd}_3\text{As}_2$  [25]

$$H(\mathbf{k}) = \hbar v_F(\sigma^x s^z k_x - \sigma^y k_y) + m(\mathbf{k})\sigma^z + \mathcal{O}(|\mathbf{k}|^2) \quad (1)$$

with  $m(\mathbf{k}) = (m_0 - m_1 k_z^2) - m_2(k_x^2 + k_y^2)$ , where  $s^{x,y,z}$  and  $\sigma^{x,y,z}$  are Pauli matrices acting on the spin and orbital parity degrees of freedom, respectively.  $\mathcal{O}(|\mathbf{k}|^2)$  is a higher-order term in momentum related to the rotational symmetries of the crystal structures, which, in the vicinity of the gap-closing points, is negligible. Therefore,

$[s^z, H(\mathbf{k})] = 0$ , and the Hamiltonian separates into two independent  $2 \times 2$  blocks, which can be labelled by the eigenvalues of  $s^z$ , namely,  $s = \pm 1$ . Each spin block contributes a Weyl node at the DPs  $\mathbf{k}_w^x = (0, 0, \chi\sqrt{m_0/m_1})$ , where  $\chi = \pm 1$  refer to the  $\mathbb{Z}_2$  charges of the DPs.

Consider the topological Dirac semimetal subjected to an electromagnetic field, which can be described by the Hamiltonian  $H(\mathbf{k} + e\mathbf{A}(\mathbf{r})/\hbar)$ , where  $\mathbf{A}(\mathbf{r})$  is a vector potential for the electromagnetic field. In a uniform magnetic field applied along the  $z$  direction, i.e.,  $\mathbf{A}(\mathbf{r}) = Bx\hat{e}_y$ , the energy spectrum can be solved exactly, yielding  $E_{n,k_z}^s = -sm_2/\ell_B^2 + \varepsilon_{n,k_z}^s$  with

$$\varepsilon_{n,k_z}^s = \begin{cases} s(\Lambda_0 - m_1 k_z^2) & n = 0 \\ \text{sgn}(n)\sqrt{(\Lambda_n - m_1 k_z^2)^2 + 2|n|(\hbar\omega_c)^2} & n \neq 0 \end{cases}, \quad (2)$$

where  $\Lambda_n = m_0 - 2|n|m_2/\ell_B^2$ ,  $\omega_c = v_F/\ell_B$  and  $\ell_B = \sqrt{\hbar/eB}$ . The Landau levels (LLs) are plotted in Figs. 1(a) and (d), each of which has a degeneracy equal to  $1/2\pi\ell_B^2$  per unit cross section. Notice that, due to the coupling between the magnetic field and the electron orbital angular momentum, a spin-dependent term  $-sm_2/\ell_B^2$  appears in the spectrum, which shifts the energies of the Weyl fermions of opposite spins in opposite directions, and thus lifts the spin degeneracy.

As we focus on the physics around the gap-closing points, it is convenient to expand Eq. (2) near the Weyl nodes. To linear order, we obtain

$$\varepsilon_{s,n}^x(q_z) = \text{sgn}(n)\hbar\sqrt{2|n|\omega_c^2 + \tilde{v}_F^2 q_z^2} + s\chi\hbar\tilde{v}_F q_z \delta_{n,0}, \quad (3)$$

where  $\tilde{v}_F = 2\hbar^{-1}\sqrt{m_0 m_1}$  and  $\mathbf{q} = \mathbf{k} - \mathbf{k}_w^x$  is momentum measured from the Weyl nodes. As it shows, in each Weyl valley, the  $n = 0$  LL is chiral, manifesting the chirality of the Weyl node, and all  $n \neq 0$  LLs are achiral. In the presence of an electric field, the system will exhibit the chiral anomaly[28, 29], i.e., the acceleration of the fermions by the electric field creates a chirality population imbalance between the Weyl valleys, and then leads to a measurable positive LMC. Here, the chiral  $n = 0$  LLs are not only  $\mathbb{Z}_2$ - but also spin-resolved. Moreover, for a single pair of Weyl nodes for a fixed spin  $s$ , the  $\mathbb{Z}_2$  charge  $\chi$  in Eq. (3) plays the role of the chirality, which exhibits the  $\mathbb{Z}_2$  quantum anomaly. The chirality manifested in the  $n = 0$  LL, in fact, can be understood as follows. The  $\mathbb{Z}_2$  charge of the DP is defined as  $\chi = (C_{\uparrow}^x - C_{\downarrow}^x)/2$ , where  $C_{\uparrow,\downarrow}^x$  are the chiralities of the spin- $\uparrow$  and spin- $\downarrow$  Weyl fermions at the  $\chi$  DP [7, 8]. The paired Weyl nodes possess opposite chiralities  $C_s^x = -C_s^{-x}$ , and therefore, the chirality of each Weyl node here is  $C_s^x = s\chi$ , which is exactly the sign of the  $n = 0$  LL's group velocity, as shown in Eq. (3). Recalling the mechanism of the positive LMC in Weyl semimetals [20], the  $\mathbb{Z}_2$  anomaly may also contribute a measurable physical quantity, which is similar to the chiral anomaly in response to the parallel electric and magnetic fields.

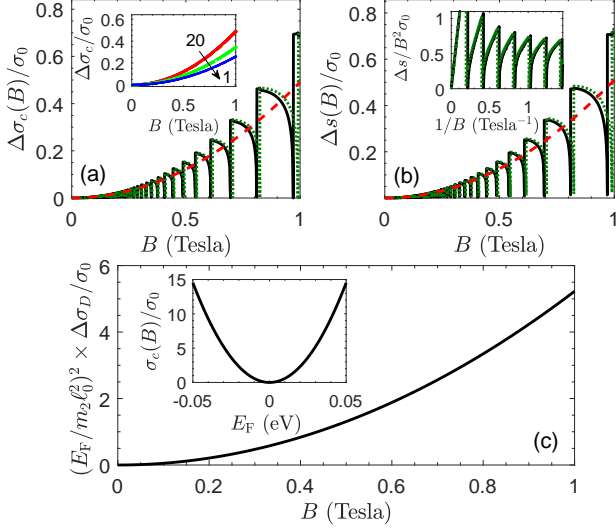


FIG. 2. (a)  $\Delta\sigma_c(B)$ , (b)  $\Delta s(B)$  and (c)  $\Delta\sigma_D$  vs the magnetic field  $B$ . The dark-solid and cyan-dotted lines in (a) and (b) stand for the spin- $\uparrow$  and spin- $\downarrow$  components, where the red-dashed lines indicate the envelopes of the oscillations, described by the classical formula in Refs. [30, 31]. The solid lines in the inset of (a) shows the envelopes of the LMC for different magnetic doping concentration, with red, green and blue for  $\tau_{\text{intra}}^s/\tau_{\text{inter}}^c = (20, 2, 1)$ . The data of (b) are replotted in its inset to show the periodic-in- $1/B$  dependence of  $\Delta s(B)$ , and the inset of (c) displays the Drude conductivity as a function of the Fermi level. Here,  $E_F = 0.03$  eV corresponding to the pink dashed lines in Fig. 1,  $\tau_{\text{intra}}^s/\tau_{\text{inter}}^c = 20$ , and  $\sigma_0 = (e^2/h)\tilde{\nu}_F\tau_{\text{intra}}/\ell_0^2$  is chosen as the unit of conductivity for convenience.

To demonstrate this effect, let us couple an external field, e.g., an electric field  $\nabla\mu_s = -e\mathbf{E}$  or a spin-dependent electric field  $\nabla\mu_s = -es\mathbf{E}$  which can be induced by a spin bias, to the fermions. Upon application of the external field, the linear-response electron distribution function in general takes the form

$$f_{s,n}^X(\mathbf{k}) = f_0(E_{n,k_z}^s) + \left[ -\frac{\partial f_0(\varepsilon_{s,n}^X)}{\partial \varepsilon_{s,n}^X} \right] g_{s,n}^X(\mathbf{k}), \quad (4)$$

where  $g_{s,n}^X(\mathbf{k})$  describes the deviation of  $f_{s,n}^X(\mathbf{k})$  from the electron equilibrium distribution function  $f_0(\varepsilon_{s,n}^X) = 1/[1 + \exp(\frac{\varepsilon_{s,n}^X - E_F^s}{k_B T})]$ , with  $E_F^s = E_F + sm_2/\ell_B^2$ . In the relaxation time approximation, the steady-state Boltzmann equation for the multiple Fermi pocket system can be expressed as [32–35]

$$\mathbf{v}_{s,n}^X \cdot \nabla\mu_s = \sum_{s'\chi'} \frac{g_{s,n}^X - \bar{g}_{ss'}^{\chi\chi'}}{\tau_{s,s'}^{\chi,\chi'}}, \quad (5)$$

where  $\bar{g}_{ss'}^{\chi\chi'} = (\bar{g}_{s,\chi} + \bar{g}_{s',\chi'})/2$  denotes the equilibrium established between the Fermi pockets and  $\tau_{s,s'}^{\chi,\chi'}$  represents the relaxation time due to disorder. The group

velocities for the LLs, given by  $\hbar\mathbf{v}_{s,n}^X = \nabla_{\mathbf{q}}\varepsilon_{s,n}^X(q_z)$ , correspond to the slopes of the dispersion and the average  $\bar{g}_{s,\chi} = \langle g_{s,n}^X(\mathbf{k}) \rangle_{s,\chi}$  is defined as

$$\langle \dots \rangle_{s,\chi} = \frac{\sum_{n,q_y} \int dq_z (\dots) \left[ -\frac{\partial f_0(E_{n,k_z}^s)}{\partial \varepsilon_{s,n}^X} \right]}{\sum_{n,q_y} \int dq_z \left[ -\frac{\partial f_0(E_{n,k_z}^s)}{\partial \varepsilon_{s,n}^X} \right]}, \quad (6)$$

where the summation runs over all electron states at the Fermi pocket in the  $\chi$  valley of  $s$  spin component. It is assumed  $\tau_{s,s}^{\chi,-\chi}, \tau_{s,-s}^{\chi,\chi}, \tau_{s,-s}^{\chi,-\chi} \gg \tau_{s,s}^{\chi,\chi}$ , based on the fact that, on one hand, the separation of the Weyl nodes usually makes the intervalley scattering much weaker than intravalley scattering, and on the other hand, the  $z$  component of the spin, served as a conserved quantity, will have a long relaxation time for dilute magnetically doping. For the sake of brevity, we denote  $\tau_{\text{intra}} = \tau_{s,s}^{\chi,\chi}$  ( $\tau_{\text{intra}}^s = \tau_{s,-s}^{\chi,\chi}$ ) and  $\tau_{\text{inter}} = \tau_{s,s}^{\chi,-\chi}$  ( $\tau_{\text{inter}}^s = \tau_{s,-s}^{\chi,-\chi}$ ) as intra-Dirac-valley and inter-Dirac-valley relaxation times due to charged (magnetic) impurity scattering.

*Electric field induced chiral chemical potential*- For  $\nabla\mu_s = -e\mathbf{E}$ , the fermions in the two spin components are accelerated by the electric field toward the same direction. Since the chiral  $n = 0$  LLs depend not only on the  $\mathbb{Z}_2$  charge  $\chi$  but also on the spin  $s$ , the spin- $\uparrow$  Weyl fermions are pumped from the negative to the positive chirality, while it reverses for the spin- $\downarrow$  Weyl fermions, indicated by the dark and red arrows in Fig. 1(a). As a result, the global equilibrium can be established by electron scattering between Weyl valleys residing at distinct or identical DPs, which includes two different relaxation processes: (i) identical spin component but different  $\mathbb{Z}_2$  charges and (ii) identical  $\mathbb{Z}_2$  charge but different spin components. In this case, we can reduce Eq. (5) to

$$e\mathbf{E} \cdot \mathbf{v}_{s,n}^X = -\frac{g_{s,n}^X - \bar{g}_{s,\chi}}{\tau_{\text{intra}}} - \frac{g_{s,n}^X - \bar{g}_s}{\tau_{\text{inter}}} - \frac{g_{s,n}^X - \bar{g}_c}{\tau_{\text{intra}}^s} \quad (7)$$

with  $\bar{g}_s = (\bar{g}_{s,\chi} + \bar{g}_{s,-\chi})/2$  and  $\bar{g}_c = (\bar{g}_{s,\chi} + \bar{g}_{-s,\chi})/2$ . For  $\tau_{\text{inter}}^c, \tau_{\text{intra}}^s \gg \tau_{\text{intra}}$ , we can approximate  $g_{s,n}^X \simeq \bar{g}_{s,\chi}$  in the last two terms of Eq. (7), and thus arrive at  $g_{s,n}^X = -e\mathbf{E} \cdot \mathbf{v}_{s,n}^X \tau_{\text{intra}} + \bar{g}_{s,\chi}$  with

$$\bar{g}_{s,\chi} = -e\mathbf{E} \cdot \langle \mathbf{v}_{s,n}^X \rangle_{s,\chi} \frac{\tau_{\text{inter}}^c \tau_{\text{intra}}^s}{\tau_{\text{inter}}^c + \tau_{\text{intra}}^s}, \quad (8)$$

where  $m_2$ ,  $\tau_{\text{intra}}/\tau_{\text{inter}}^c$  and  $\tau_{\text{intra}}/\tau_{\text{intra}}^s$  are dropped first due to smallness. It is noticed that only the chiral  $n = 0$  LLs make a nonzero contribution to  $\langle \mathbf{v}_{s,n}^X \rangle_{s,\chi}$  and, in turn, to  $\bar{g}_{s,\chi}$ . As  $\mathbf{v}_{s,0}^X \propto s\chi$ , the sign of  $\langle \mathbf{v}_{s,n}^X \rangle_{s,\chi}$  is determined by the product of  $s$  and  $\chi$ . According to Eq. (4),  $\bar{g}_{s,\chi}$  in fact corresponds to the nonequilibrium local chemical potential in the Weyl valleys. Therefore, we define the chiral chemical potential for each spin component as  $\Delta\mu_s = (\bar{g}_{s,+} - \bar{g}_{s,-})/2$ . The chiral chemical potentials for the two spin components are equal in

magnitude but opposite in the signs, as shown in Figs. 1(a)-(c). For dilute magnetically doping  $\tau_{\text{intra}}^s \gg \tau_{\text{inter}}^c$ ,  $\Delta\mu_s = -e\chi\mathbf{E} \cdot \langle \mathbf{v}_{s,n}^\chi \rangle_{s,\chi} \tau_{\text{inter}}^c$ , which recovers the result for Weyl semimetals of a single pair of nodes [20]. Here, as the magnetic impurity scattering strengthens, the chiral chemical potential will reduce quickly, as indicated by Eq. (8). With further increasing the magnetic doping concentration,  $\tau_{\text{intra}}^s < \tau_{\text{inter}}^c$  could be accessible, and then the chiral chemical potentials turns to be very sensitive to the local magnetic disorder.

*Spin bias induced  $\mathbb{Z}_2$  chemical potential*- For  $\nabla\mu_s = -es\tilde{\mathbf{E}}$ , the Weyl fermions in the two spin components are accelerated toward opposite directions, such that the global equilibrium can only be established by electron scattering between different DPs. In this situation, Eq. (5) reduces to be

$$es\tilde{\mathbf{E}} \cdot \mathbf{v}_{s,n}^\chi = -\frac{g_{s,n}^\chi - \bar{g}_{s,\chi}}{\tau_{\text{intra}}} - \frac{g_{s,n}^\chi - \bar{g}_s}{\tau_{\text{inter}}^c} - \frac{g_{s,n}^\chi - \bar{g}_z}{\tau_{\text{inter}}^s} \quad (9)$$

with  $\bar{g}_z = (\bar{g}_{s,\chi} + \bar{g}_{-s,-\chi})/2$ . From Eq. (9), we obtain for

$$\bar{g}_{s,\chi} = -es\tilde{\mathbf{E}} \cdot \langle \mathbf{v}_{s,n}^\chi \rangle_{s,\chi} \frac{\tau_{\text{inter}}^c \tau_{\text{inter}}^s}{\tau_{\text{inter}}^c + \tau_{\text{inter}}^s}. \quad (10)$$

As analyzed above,  $\bar{g}_{s,\chi}$  now is only  $\chi$ -dependent and the chemical potential difference  $\Delta\mu_z = (\bar{g}_{s,+} - \bar{g}_{s,-})/2$  becomes spin-independent. Therefore, upon application of the spin bias, the fermion population decreases in the left DP and increases in the right, as illustrated in Fig. 1(d). The overall effect of this process is that the Dirac fermions are pumped from one DP to the other, which exhibits the  $\mathbb{Z}_2$  anomaly. Consequently, we dub  $\Delta\mu_z$  the  $\mathbb{Z}_2$  chemical potential. A nonzero  $\Delta\mu_z$  presented in Figs. 1(d)-(f) indicates that an imbalance of carrier density is established between the two DPs. Usually, the spin-flip inter-Dirac-valley relaxation is much slower than the other relaxation processes and thus, the  $\mathbb{Z}_2$  chemical potential is insensitive to the local magnetic disorder.

*Positive LMC and LSMC*- The spin-dependent current density is given by

$$\mathbf{j}_s = \frac{e}{2\pi} \sum_{\chi} \sum_{n,k_y} \int g_{s,n}^\chi(\mathbf{k}) \mathbf{v}_{s,n}^\chi \left[ \frac{\partial f_0(\varepsilon_{s,n}^\chi)}{\partial \varepsilon_{s,n}^\chi} \right] dk_z \quad (11)$$

with  $g_{s,n}^\chi(\mathbf{k}) = \nabla\mu_s \cdot \mathbf{v}_{s,n}^\chi \tau_{\text{intra}} + \bar{g}_{s,\chi}$ . Incorporating the chiral and  $\mathbb{Z}_2$  anomalies, together with  $\sum_{s,\chi} \bar{g}_{s,\chi} = 0$  due to particle conservation of the system, we average both sides of Eq. (5) at the Fermi level and obtain

$$\bar{g}_{s,\chi} = -s\chi\tilde{P}_- \frac{\tau_{\text{inter}}^c \tau_{\text{intra}}^s}{\tau_{\text{inter}}^c + \tau_{\text{intra}}^s} + \chi\tilde{P}_+ \frac{\tau_{\text{inter}}^c \tau_{\text{inter}}^s}{\tau_{\text{inter}}^c + \tau_{\text{inter}}^s}, \quad (12)$$

where

$$\tilde{P}_\pm = \frac{\nabla\mu_- \cdot \langle \mathbf{v}_{-,n}^+ \rangle_{-,+} \pm \nabla\mu_+ \cdot \langle \mathbf{v}_{+,n}^+ \rangle_{+,+}}{2}. \quad (13)$$

At low temperatures, one can further derive  $\langle \mathbf{v}_{s,n}^\chi \rangle_{s,\chi} = s\chi\tilde{v}_F/\Theta_s$ , with  $\Theta_s = 2 \sum_{n=0}^{n_c} \frac{1}{\lambda_{n,s}} - 1$ , where  $\lambda_{n,s} = \sqrt{1 - 2|n|(\frac{\hbar\omega_c}{E_F^s})^2}$  and  $n_c = \text{sgn}(E_F) \text{int}[(E_F^s/2)^2/(\hbar\omega_c)^2]$  is level index of the highest (lowest) LL crossed by the Fermi level for  $E_F > 0$  ( $E_F < 0$ ). To see the physical meaning of  $\tilde{P}_\pm$  more clearly, we set  $m_2 = 0$  and then  $\Theta_s$  is spin-independent. For  $\nabla\mu_s = -e\mathbf{E}$ ,  $\tilde{P}_+ = 0$  and Eq. (12) returns to Eq. (8), while for  $\nabla\mu_s = -es\tilde{\mathbf{E}}$ ,  $\tilde{P}_- = 0$  and Eq. (12) recovers Eq. (10). Therefore,  $|\tilde{P}_\pm|$  in fact describes the effective power of the particle pumping between the DPs.

Substituting Eq. (12) into Eq. (11), we can express the spin-dependent current density as

$$j_{s,z}(B) = \sigma_D^s(E_z + s\tilde{E}_z) + \Delta\sigma(B) \times \left( \frac{\tau_{\text{intra}}^s}{\tau_{\text{inter}}^c + \tau_{\text{intra}}^s} E_z + \frac{\tau_{\text{inter}}^s}{\tau_{\text{inter}}^c + \tau_{\text{inter}}^s} s\tilde{E}_z \right), \quad (14)$$

where  $\sigma_D^s = \frac{e^2 n_{c,s}^s}{\hbar k_{F,s}} \tilde{v}_F \tau_{\text{intra}}$  is the Drude conductivity with  $k_{F,s} = |E_F^s|/\hbar\tilde{v}_F$  and  $n_{c,s}^s = (1/3\pi^2)k_{F,s}^3$  as the spin-resolved carrier density, and

$$\Delta\sigma(B) = \frac{e^2}{h} \frac{eB\tilde{v}_F\tau_{\text{inter}}^c}{h} \sum_s \frac{1}{\Theta_s} \quad (15)$$

is the magnetoconductivity attributable to the nonequilibrium local chemical potentials. Equations (14) is the central result of our work, from which we define the spin-resolved electric and spin conductivity as  $\sigma_c(B) = j_{s,z}(B)/E_z$  and  $s(B) = j_{s,z}(B)/s\tilde{E}_z$ . The LMC for Weyl semimetals of a single pair of Weyl nodes is given by Eq. (15), which has been discussed by us in Ref. [20]. Here, the electron orbital angular momentum couples strongly with the magnetic field, and the Weyl fermions can relax via electron scattering between multiple Fermi pockets. Therefore, new characteristic will emerge in the magnetotransport. The LSMC, given by  $\Delta s(B) \equiv [s(B) - s(0)]$ , is a spin version of the LMC due to the  $\mathbb{Z}_2$  anomaly.

In Fig. 2, we plot the calculated  $\Delta\sigma_c(B) \equiv [\sigma_c(B) - \sigma_c(0)]$ ,  $\Delta s(B)$  and  $\Delta\sigma_D = \sum_s \sigma_D^s - \sigma_D$  as functions of  $B$ , where  $\sigma_D$  is the zero-field Drude conductivity. As seen from Figs. 2(a) and (b), though the Zeeman effect is neglected, the spin degeneracy of the LMC and LSMC are eliminated by the coupling of the electron orbital angular momentum and magnetic field. Due to the chiral and  $\mathbb{Z}_2$  anomalies, the LMC and LSMC exhibit synchronous oscillations with the chiral and  $\mathbb{Z}_2$  chemical potentials. The envelopes of the oscillations are scaled with  $B^2$  for  $\hbar\omega_c \ll |E_F|$ , which is consistent with the classical formula obtained in Refs. [30, 31]. From Fig. 2(c), we see that, because of the coupling between the electron orbital angular momentum and magnetic field, the trivial Drude conductivity also contributes a  $B$ -dependent term

$$\Delta\sigma_D^s/\sigma_D = \left(\frac{em_2}{\hbar E_F}\right)^2 B^2 + 2s \frac{em_2}{\hbar E_F} B \quad (16)$$



to the positive LMC, which is similar to that due to the chiral anomaly. Therefore, the  $B^2$  or  $B$  dependence emerging in the positive LMC is not unique to the chiral anomaly. However, the quantum oscillations of the LMC are originated from the chiral  $n = 0$  LLs, manifesting the chiral anomaly. As shown by Eq. (14), the LSMC possesses all characters of the chiral-anomaly-induced LMC, including the periodic-in- $1/B$  quantum oscillations, as exhibited in the inset of Fig. 2(b). While the chiral anomaly is very sensitive to the local magnetic impurities, please see the inset of Fig. 2(a), the  $\mathbb{Z}_2$  anomaly is immune to local magnetic disorder.

In conclusion, we have theoretically studied the anomalous magnetotransports in Dirac semimetals carrying the  $\mathbb{Z}_2$  topological charge. We find that a spin bias along the magnetic field can realize the  $\mathbb{Z}_2$  anomaly for topological Dirac semimetals. Accompanied with this, there emerges a measurable positive LSMC. We further demonstrate that the  $B^2$  and  $B$  dependences of the positive LMC are not unique to the chiral anomaly, because similar field dependences can also originate from the coupling between the electron orbital angular momentum and magnetic field. The  $\mathbb{Z}_2$  anomaly induced LSMC possesses all characters of the LMC due to the chiral anomaly, and we argue that the periodic-in- $1/B$  quantum oscillations superposed on the positive LSMC can serve as a fingerprint of the  $\mathbb{Z}_2$  anomaly in topological Dirac semimetals.

This work was supported by the National Natural Science Foundation of China under Grants No. 11674160 (L.S.), 11874016 (R.-Q.W), 11804130 (W.L.) and 11574155 (R.M.), by the Key Program for Guangdong NSF of China under Grant No. 2017B030311003, GDUPS(2017) and the project funded by South China Normal University under Grant No. 671215 and 8S0532.

---

\* wangruiqiang@m.scnu.edu.cn

† shengli@nju.edu.cn

- [1] N. P. Armitage, E. J. Mele, and A. Vishwanath, *Rev. Mod. Phys.* **90**, 015001 (2018).
- [2] Z. K. Liu, B. Zhou, Y. Zhang, Z. J. Wang, H. M. Weng, D. Prabhakaran, S.-K. Mo, Z. X. Shen, Z. Fang, X. Dai, Z. Hussain, and Y. L. Chen, *Science* **343**, 864 (2014).
- [3] C.-L. Zhang, S.-Y. Xu, I. Belopolski, Z. Yuan, Z. Lin, B. Tong, G. Bian, N. Alidoust, C.-C. Lee, S.-M. Huang, T.-R. Chang, G. Chang, C.-H. Hsu, H.-T. Jeng, M. Neupane, D. S. Sanchez, H. Zheng, J. Wang, H. Lin, C. Zhang, H.-Z. Lu, S.-Q. Shen, T. Neupert, M. Zahid Hasan, and S. Jia, *Nat. Commun.* **7**, 10735 (2016).
- [4] J. Xiong, S. K. Kushwaha, T. Liang, J. W. Krizan, M. Hirschberger, W. Wang, R. J. Cava, and N. P. Ong, *Science* **350**, 413 (2015).
- [5] C. Zhang, E. Zhang, W. Wang, Y. Liu, Z.-G. Chen, S. Lu, S. Liang, J. Cao, X. Yuan, L. Tang, Q. Li, C. Zhou, T. Gu, Y. Wu, J. Zou, and F. Xiu, *Nat. Commun.* **8**, 13741 (2017).
- [6] C. M. Wang, H.-P. Sun, H.-Z. Lu, and X. C. Xie, *Phys. Rev. Lett.* **119**, 136806 (2017).
- [7] B.-J. Yang and N. Nagaosa, *Nat. Commun.* **5**, 4898 (2014).
- [8] E. V. Gorbar, V. A. Miransky, I. A. Shovkovy, and P. O. Sukhachov, *Phys. Rev. B* **91**, 121101 (2015).
- [9] M. Kargarian, M. Randeria, and Y.-M. Lu, *Proceedings of the National Academy of Sciences* **113**, 8648 (2016).
- [10] S. Raza, A. Sirota, and J. C. Y. Teo, *Phys. Rev. X* **9**, 011039 (2019).
- [11] A. A. Zyuzin, S. Wu, and A. A. Burkov, *Phys. Rev. B* **85**, 165110 (2012).
- [12] P. Goswami and S. Tewari, *Phys. Rev. B* **88**, 245107 (2013).
- [13] S. Han, G. Y. Cho, and E.-G. Moon, *Phys. Rev. B* **98**, 085149 (2018).
- [14] M.-X. Deng, W. Luo, R.-Q. Wang, L. Sheng, and D. Y. Xing, *Phys. Rev. B* **96**, 155141 (2017).
- [15] C. Chen, Z.-M. Yu, S. Li, Z. Chen, X.-L. Sheng, and S. A. Yang, *Phys. Rev. B* **99**, 075131 (2019).
- [16] H. Nielsen and M. Ninomiya, *Physics Letters B* **130**, 389 (1983).
- [17] G. E. Volovik, *The universe in a helium droplet*, Vol. 117 (Oxford University Press on Demand, 2003).
- [18] X. Wan, A. M. Turner, A. Vishwanath, and S. Y. Savrasov, *Phys. Rev. B* **83**, 205101 (2011).
- [19] X. Huang, L. Zhao, Y. Long, P. Wang, D. Chen, Z. Yang, H. Liang, M. Xue, H. Weng, Z. Fang, X. Dai, and G. Chen, *Phys. Rev. X* **5**, 031023 (2015).
- [20] M.-X. Deng, G. Y. Qi, R. Ma, R. Shen, R.-Q. Wang, L. Sheng, and D. Y. Xing, *Phys. Rev. Lett.* **122**, 036601 (2019).
- [21] S. Liang, J. Lin, S. Kushwaha, J. Xing, N. Ni, R. J. Cava, and N. P. Ong, *Phys. Rev. X* **8**, 031002 (2018).
- [22] M. Neupane, S.-Y. Xu, R. Sankar, N. Alidoust, G. Bian, C. Liu, I. Belopolski, T.-R. Chang, H.-T. Jeng, H. Lin, A. Bansil, F. Chou, and M. Z. Hasan, *Nat. Commun.* **5**, 3786 (2014).
- [23] C.-Z. Li, L.-X. Wang, H. Liu, J. Wang, Z.-M. Liao, and D.-P. Yu, *Nat. Commun.* **6**, 10137 (2015).
- [24] Z. Wang, Y. Sun, X.-Q. Chen, C. Franchini, G. Xu, H. Weng, X. Dai, and Z. Fang, *Phys. Rev. B* **85**, 195320 (2012).
- [25] Z. Wang, H. Weng, Q. Wu, X. Dai, and Z. Fang, *Phys. Rev. B* **88**, 125427 (2013).
- [26] A. A. Burkov and Y. B. Kim, *Phys. Rev. Lett.* **117**, 136602 (2016).
- [27] C. M. Wang, H.-Z. Lu, and S.-Q. Shen, *Phys. Rev. Lett.* **117**, 077201 (2016).
- [28] A. A. Zyuzin and A. A. Burkov, *Phys. Rev. B* **86**, 115133 (2012).
- [29] A. V. Andreev and B. Z. Spivak, *Phys. Rev. Lett.* **120**, 026601 (2018).
- [30] D. T. Son and B. Z. Spivak, *Phys. Rev. B* **88**, 104412 (2013).
- [31] X. Xiao, K. T. Law, and P. A. Lee, *Phys. Rev. B* **96**, 165101 (2017).
- [32] S. Hershfield and V. Ambegaokar, *Phys. Rev. B* **34**, 2147 (1986).
- [33] K.-S. Kim, H.-J. Kim, and M. Sasaki, *Phys. Rev. B* **89**, 195137 (2014).
- [34] K. Das and A. Agarwal, *Phys. Rev. B* **99**, 085405 (2019).
- [35] M.-X. Deng, H.-J. Duan, W. Luo, W. Y. Deng, R.-Q. Wang, and L. Sheng, *Phys. Rev. B* **99**, 165146 (2019).